Laser-Produced Plasma Light Source for EUVL

Igor V. Fomenkov*, David C. Brandt, Alexander N. Bykanov, Alex I. Ershov, William N. Partlo, David W. Myers, Norbert R. Böwering, Nigel R. Farrar, Georgiy O. Vaschenko, Oleh V. Khodykin, Jerzy R. Hoffman, Christopher P. Chrobak, Shailendra N. Srivastava, Daniel J. Golich, David A. Vidusek, Silvia De Dea, Richard R. Hou

Cymer Inc., 17075 Thornmint Court, San Diego, CA, 92127, USA

ABSTRACT

This paper is devoted to the development of laser produced plasma (LPP) EUV source architecture for advanced lithography applications in high volume manufacturing of integrated circuits. The paper describes the development status of subsystems most critical to the performance to meet scanner manufacturer requirements for power and debris mitigation. Spatial and temporal distributions of the radiation delivered to the illuminator of the scanner are important parameters of the production EUV tool, this paper reports on these parameters measured at the nominal repetition rate of the EUV source. The lifetime of the collector mirror is a critical parameter in the development of extreme ultra-violet LPP lithography sources. Deposition of target material and contaminants as well as sputtering and implantation of incident particles can reduce the reflectivity of the mirror coating substantially over time during exposure even though debris mitigation schemes are being employed. We report on progress of life-test experiments of exposed 1.6sr collectors using a Sn LPP EUV light source. The erosion of MLM coating is caused mostly by the high-energy ions generated from the plasma. In this manuscript the ion distribution measured at small (14 degree) and medium (45 degree) angles to the laser beam are presented. The measurements show that the chosen combination of the CO_2 laser and Sn droplet targets is characterized by fairly uniform angular ion energy distribution. The maximum ion energy generated from the plasma is in the range of 3-3.5 keV for all incident angles of the collector. The measured maximum energy of the ions is significantly less than that measured and simulated for plasmas generated by short wavelength lasers (1 μm). The separation of ions with different charge states was observed when a retarding potential was applied to the Faraday Cup detector.

Keywords: EUV source, EUV lithography, Laser Produced Plasma, Collector, Plasma

1. INTRODUCTION

EUV lithography is expected to follow 193 nm immersion lithography for critical layer imaging in the sub-32nm era. Laser produced plasma (LPP) sources have emerged as the leading technology to enable high power production with scalability toward the future. The high conversion efficiency (CE) of CO_2 drive laser and Sn target material enables the required EUV power levels for high volume manufacturing (HVM) to be achieved at relatively low laser power so that cost of operation can be kept to a minimum. Drive laser power is scalable through increase of repetition rate and pulse energy making the technology easily extendable to even higher powers for future generations of EUV scanners, or enabling compensation for photoresist sensitivity limitations. The isolated plasma in the central region of the source chamber provides large distances between the hot plasma and chamber components. There are no electrodes, hence there is no need for elaborate and expensive electrode cooling, nor is there any electrode debris as observed in discharge produced plasma (DPP) sources. The small etendue of an LPP source reduces the complexity of optical system designs and supports illuminators with variable sigma and advanced illumination techniques such as annular, dipole, or quadrupole. Normal Incidence (NI) collector mirrors exhibit greater thermal load capacity and greater image fidelity under high heat load compared to grazing incidence collectors employed in DPP systems. The multi-layer (ML) coating provides substantial spectral filtering of out-of-band (OOB) EUV radiation. In addition, the ML coating can be stacked, or the number of layer periods can be increased, providing sacrificial layers that extend the useful lifetime of the NI collector and enable a low-cost operation of the source in a HVM environment. The goal of our development efforts is to provide a cost-effective high-power LPP EUV light source that meets requirements for production EUV lithography in the post-193 nm era,

Alternative Lithographic Technologies, edited by Frank M. Schellenberg, Bruno M. La Fontaine
Proc. of SPIE Vol. 7271, 727138 · © 2009 SPIE · CCC code: 0277-786X/09/$18 · doi: 10.1117/12.814272

as described in the joint specifications of the exposure tool manufacturers[1], and for integration with specific designs of individual lithography customers.

Igor V. Fomenkov; ifomenkov@cymer.com

2. SYSTEM DESCRIPTION WITH CONTROL SUBSYSTEMS

The source chamber of our development life-test system (LT1) is shown in Figure 1 and schematically in Figure 2. It is accompanied by a pulsed high power CO_2 laser system operating at a wavelength of 10.6 microns and a repetition rate of about 50 kHz.[2] The laser beam enters the vacuum chamber through an entrance window and is focused onto the target through a central hole in the collector mirror. The focusing system is highly accurate with active beam steering, producing a beam waist at the target site of approximately 150 microns in diameter. The target site is located at the primary focus of an elliptical collector optic with the other focus, called Intermediate Focus (IF), located at the region of the interface with the scanner. A vertically oriented liquid tin (Sn) droplet generator is positioned at the top of the chamber. It produces droplet sizes from 30 to 50 microns in diameter at repetition rates of about 50 kHz. Droplet speed capability is in excess of 30 meters per second with inter-droplet timing stability better than 0.2 % of the period. Unexposed droplets are caught and disposed off in a droplet catcher system. Droplet position in X and Z (Z is the CO_2 laser beam direction and X is the horizontal axis perpendicular to the laser beam) is controlled with a closed-loop steering system using a feedback signal from targeting charge coupled device (CCD) cameras. Calibrated EUV sensors positioned at several angles with respect to the X-Z plane and laser beam direction measure the 2 % bandwidth EUV energy produced by each pulse. Turbomolecular pumps are employed for evacuation of the chamber; system base pressures in the range of 10^{-6} Torr or less can be achieved.

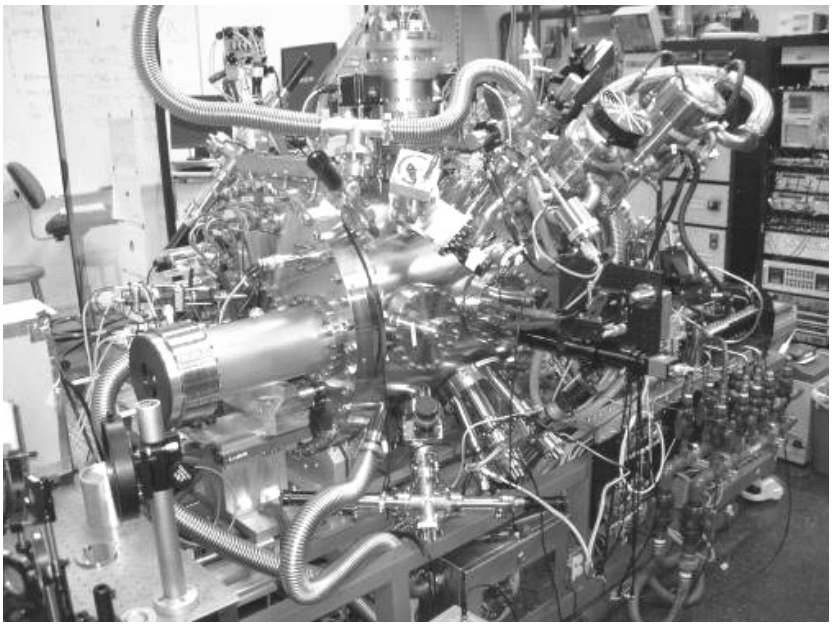

Figure 1. Photograph of LT1 development system. The source was upgraded to ~25% duty cycle operation.

When irradiated by the laser, each tin droplet is evaporated, ionized and heated to the optimal temperature where the plasma produces EUV photons most efficiently. The EUV photons emitted in the direction of the ellipsoidal mirror are collected. A multi-layer coated optic[3] covers about 1.6 steradians (>5sr on production systems) solid angle, reflecting and focusing the energy to the IF, where an aperture and several metrology devices are placed to measure the quality of light in the far field. Debris mitigation is incorporated to protect the multi-layer coating on the collector from high energy ions and other particles emitted from the plasma. Faraday cup sensors and ML mirror witness samples can be used together when mounted on a holder, replacing the collector, to measure ion energies and ion damage to the coating. In addition to visible CCD cameras for controls, we have incorporated pinhole camera devices with EUV sensitive detection to view the plasma and measure the size of the EUV emitting region.

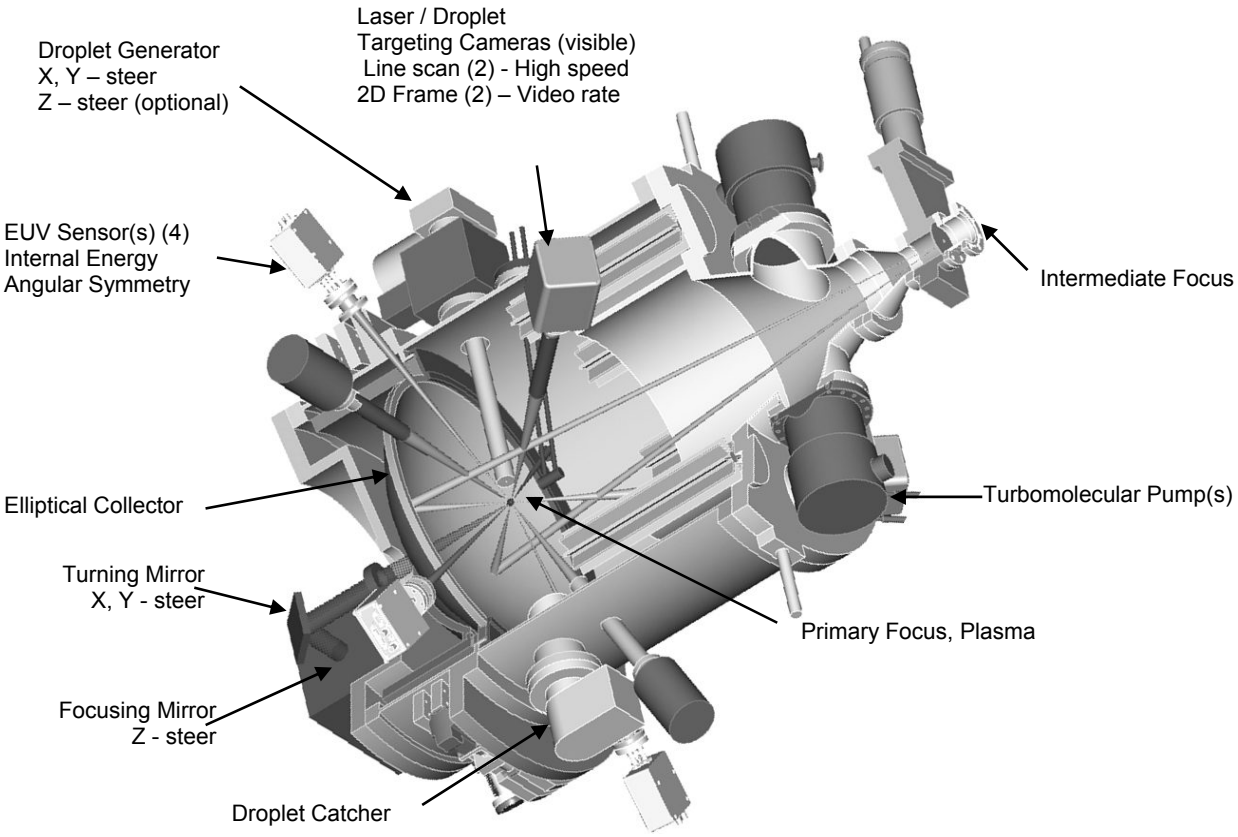

Figure 2. Drawing of EUV source chamber with associated sub-systems.

3. RECENT DEVELOPMENT RESULTS

During the course of the last year we have increased the performance characteristics of this LT1 development system significantly in comparison to previous development stages[4,5]. Some performance characteristics with respect to droplet generator stability, energy stability, EUV emission region size and source position stability were already described.[5] The duty cycle limit for continuous operation was now increased from ~10 % to about 25 % by incorporation of water cooling devices for the chamber wall. The typical duration of continuous run time could also be increased from minutes to a few hours of operation. An improved droplet position control was implemented and the droplet catching device was upgraded. Using test samples arranged in a sample holder at the position of the collection mirror or collector mirrors of 320 mm diameter with 1.6 sr collection angle, long-term tests have been carried out. Figure 3 shows the in-band EUV power obtained during an extended lifetime test run exceeding 50 hours of continuous operation at 25 % duty cycle The system was operated with 1 ms long bursts at 40 kHz repetition rate with open loop energy control. EUV power is measured at plasma and calculated for IF using the standard assumptions of 5 sr light collection with 50 % average collector reflectivity and 90 % transmission through the system. IF equivalent in-band EUV power levels of ~ 40 W were generally obtained throughout the run with only a very slow decrease over time.

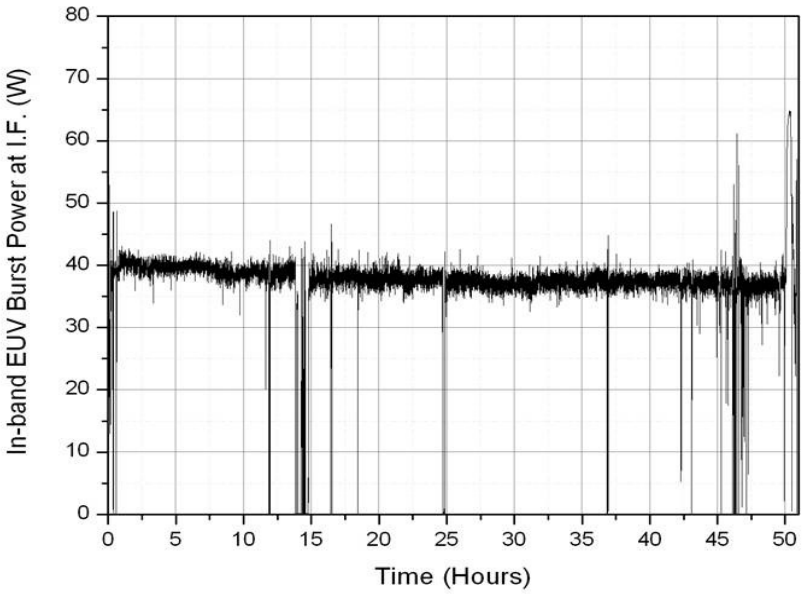

Figure 3. Lifetime test result for more than 50 hours operation time. EUV power for 1 ms bursts at 40 kHz, 25% duty cycle.

A further improvement was achieved by changing the burst pattern to a mode that is more characteristic for the intended use in the exposure tool. The burst length was increased to 400 ms duration. Figure 4 gives a comparison of CO_2 laser power and corresponding in-band EUV output power vs. time for operation in this long-duration burst mode at 40 kHz repetition rates. Typically, EUV powers in the range of 60 W are obtained in open-loop operation without energy control. A strong correlation between incident CO_2 laser power and EUV output power is observed.

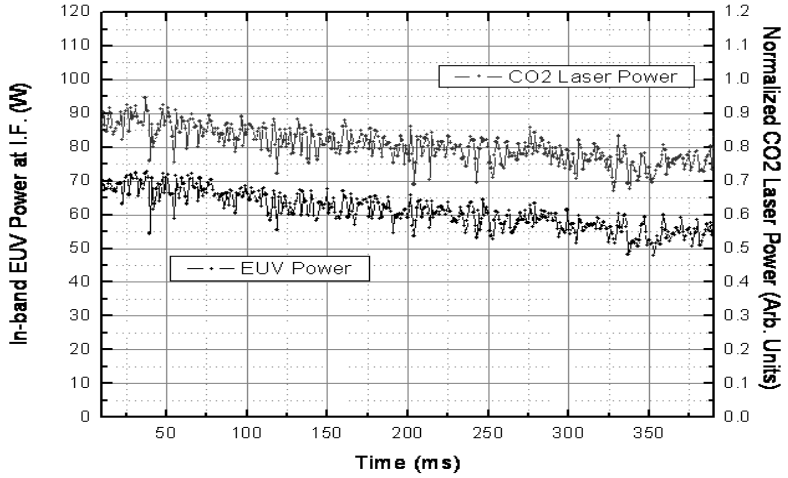

Figure 4. Normalized CO_2 laser power and in-band EUV power vs. time for 400 ms burst duration at 40 kHz. Each data point represents the integral over 40 pulses.

4. FAR FIELD METROLOGY

The IF interface represents the zone separating the source and the exposure tool. Behind the IF region several important measurements of EUV irradiation can be performed. At a distance of a few centimeters behind IF the EUV intensity distribution can be intercepted in order to obtain information on source power, the angular distribution and its stability, as well as on collector reflectance and collector defects. This plane represents a far field (FF) distribution of EUV radiation. The shape and intensity of the EUV distribution can be used for precise positioning of the source plasma in the focal point of the collector. We have developed some metrology concepts for characterization of the FF distribution. A schematic setup of our diagnostic is shown in Figure 5. A fluorescent converter screen is placed behind IF; the generated visible image is monitored with a CCD video camera behind a vacuum window. The fluorescent converter screen is composed of a Ce:YAG crystal coated with thin films of Zr (150 nm thick) and Si (25 nm thick). The transmission of the coating together with the MLM coating of collector provides a good spectral selection for EUV radiation. However, it has to be kept in mind that the radiation bandwidth after a single reflection from the collector (~4%) is wider than that of multiple reflections of further EUV optics (~2%), which gives some uncertainty to the corresponding intensity distribution into 2% bandwidth.

Two attenuators with a light transmission of 26% were installed on translational stages behind the IF aperture. The attenuators enable a reduction of the radiation incident on the fluorescent screen and thus provide the capability to measure collector images at high duty cycles. Using a fluorescent converter with a short fluorescent time (~70 ns) allows for measurements with high repetition rates.

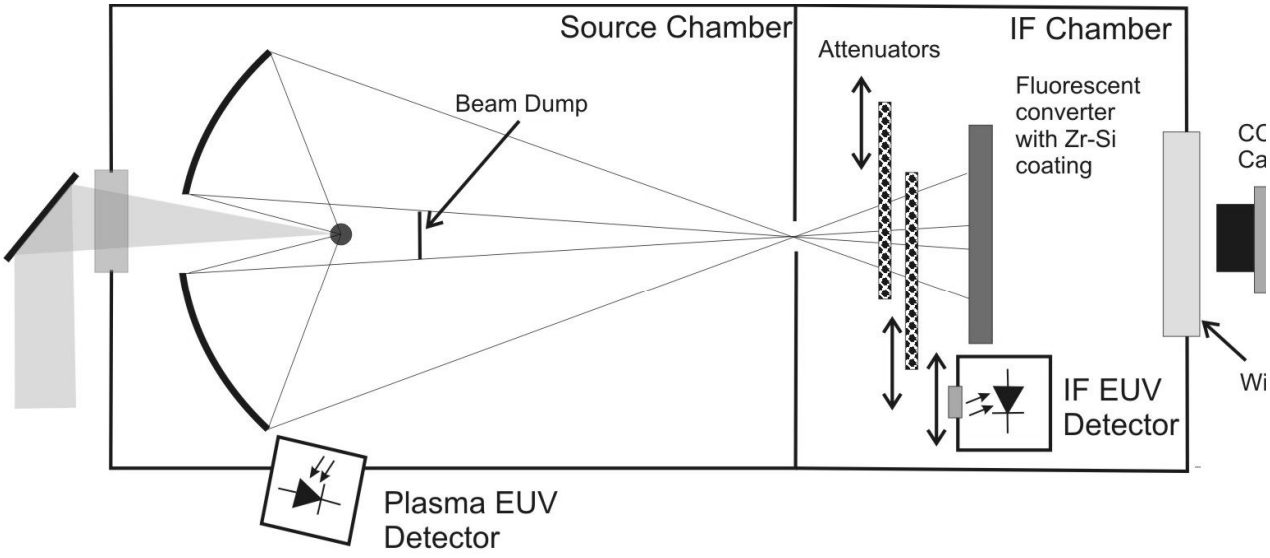

Figure 5. Schematics of diagnostic setup for far field measurements. A fluorescence converter and a CCD camera are used for image recording behind IF; attenuators can be inserted for power reduction. Photodiode-based EUV detectors are employed to determine power at plasma and converter calibration.

Figure 6 presents a typical EUV image obtained with a CCD video camera at about 26 cm behind IF at the start of an extended test run. The figure shows the fluorescent converter image of the light cone obtained within the clear aperture of the collector. Part of the image is blocked by some hardware inside of the source chamber; a large obscuration masking a horizontal section of the image was also taken into account. Some ring-shaped intensity variations are attributed to imperfections of the collector substrate. The image is divided into three different zones corresponding to different types of debris protection, as described further below. For more accurate and detailed measurements of this type, fluorescence screens of larger size can be used. Future designs will employ multiple screens with the possibility to perform measurements in the FF at distances behind IF which are significantly larger than 26 cm.

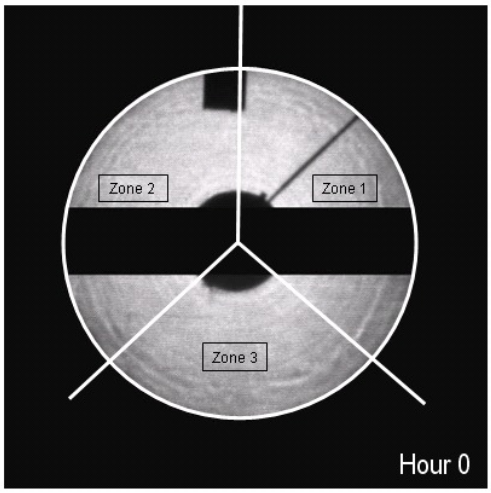

Figure 6. Far field EUV intensity distribution of collector within clear aperture at the beginning of a 51 hour longevity test. The debris protection is divided into three different zones.

The intensity distribution images were also used for quantitative EUV measurements. For this purpose we employed an insertable EUV photodiode (AXUV-100) behind a 1 μm Zr foil placed in the plane of the fluorescent converter in a well defined position (see schematics of Fig. 5). The EUV signal measured with the photodiode was attributed to the intensity of the defined image zone. The entire image intensity was then integrated with this calibration factor. The EUV energy measured behind IF in this way with the calibrated fluorescent converter was found to be in good agreement with the energy measured at plasma and projected into IF using the assumptions described above (50% average collector reflectivity and 90% transmission). Figure 7 shows the correlation between the EUV energy signals determined from the integrated image intensity and those measured from the photodiode looking directly at plasma. In the range examined the data indicate a fully linear relationship.

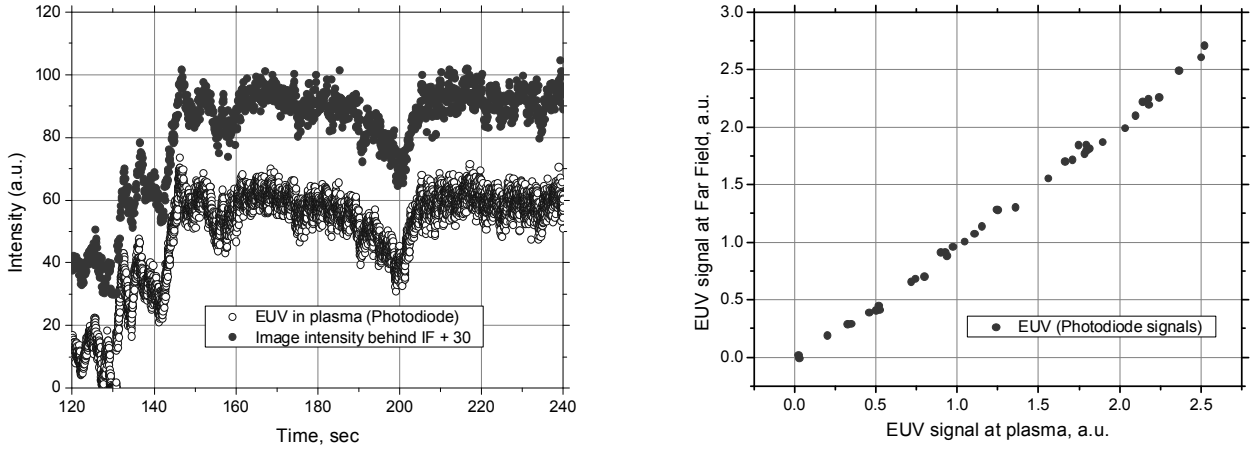

Figure 7. a) FF collector intensities obtained with a photodiode looking at the plasma and by the image detection behind IF. b) Correlation between signals measured at plasma and at far field.

Imaging the collector with the fluorescent converter after IF enabled us to monitor the collector reflectivity over time. As reported previously[5], successful continuous operation at ~ 45 W of EUV power at 8% duty cycle could be sustained for 8 hours without significant degradation of the FF image to within measurement accuracy. This test was

repeated at higher power and for a longer time, 51 hours in total at IF-equivalent power levels of ~ 40 W and at an increased duty cycle of 25 %. The FF intensity distribution at the beginning of the run is shown in Fig. 6. Figure 8 shows six FF images taken at 8 hour intervals during the course of this long run. To accelerate the testing three different variants of debris protection were used simultaneously for three zones of the collector. They are labeled as Zones 1, 2, and 3 in Fig. 6 and correspond to different protection geometries. The same labeling applies to the images of Fig. 8. As seen from the figure, in particular Zone 1, but also Zone 2 showed some degradation relatively early in the test (after a few hours) and continued to give reduced image intensity due to reflectivity decrease during the remaining hours. On the other hand, Zone 3 did not show this reduction, and no substantial change was observed until about 40 hours of exposure. Then Zone 3 began to exhibit some degradation, as well, as is shown in the 50 hours exposure image in Figure 8. However, it is believed that this reduction was in part influenced by encroachment from the neighboring Zones 1 and 2. The protection scheme corresponding to Zone 3 was thus found to be superior to the ones employed in Zones 1 and 2. Zone 3 geometries were ultimately determined to be successful and deemed suitable for the production design. The relative intensity of a 3cm x 3cm area of Zone 3 as viewed from IF with the fluorescence converter was compared to the intensity recorded by the detector monitoring EUV power at plasma. The relative collector reflectivity obtained in this way was found to stay nearly constant for the first 40 hours of the run and then to decline slightly to ~0.9 after 50 hours.

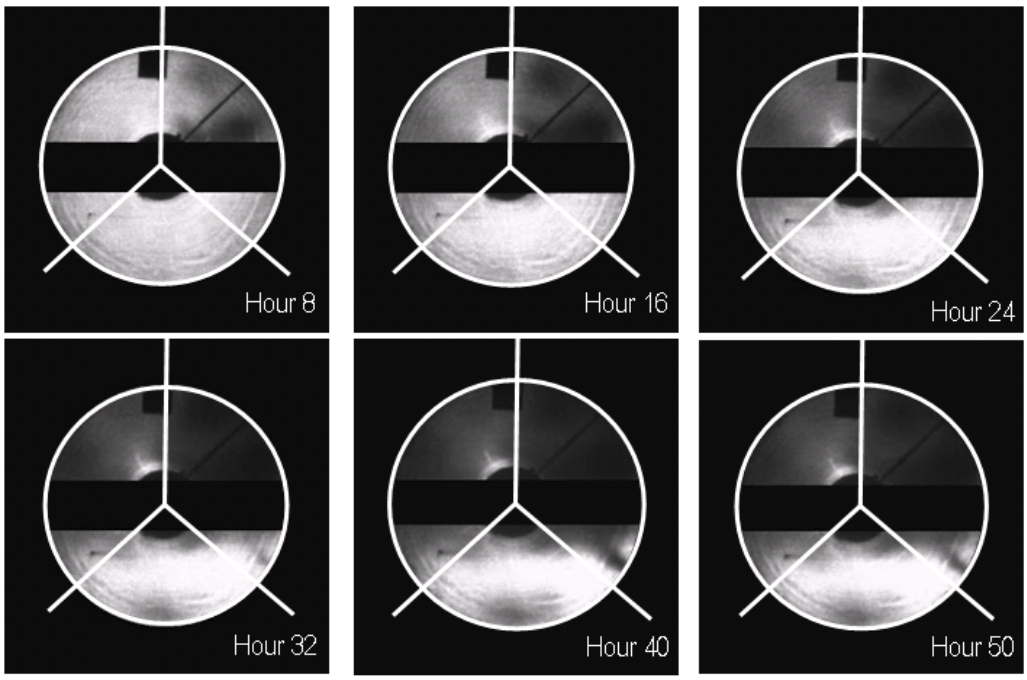

Figure 8. Evolution of far field image of sub-aperture collector over a 50 hour period. The viewing area is divided into three different zones of debris protection.

5. PLASMA PARAMETERS FOR OPTIMAL CE

For the measurements of CE, spectra, and ion energy distributions we used an experimental setup with low repetition rates. The measurements were conducted on droplets and flat targets. The arrangement is shown schematically in Figure 9.

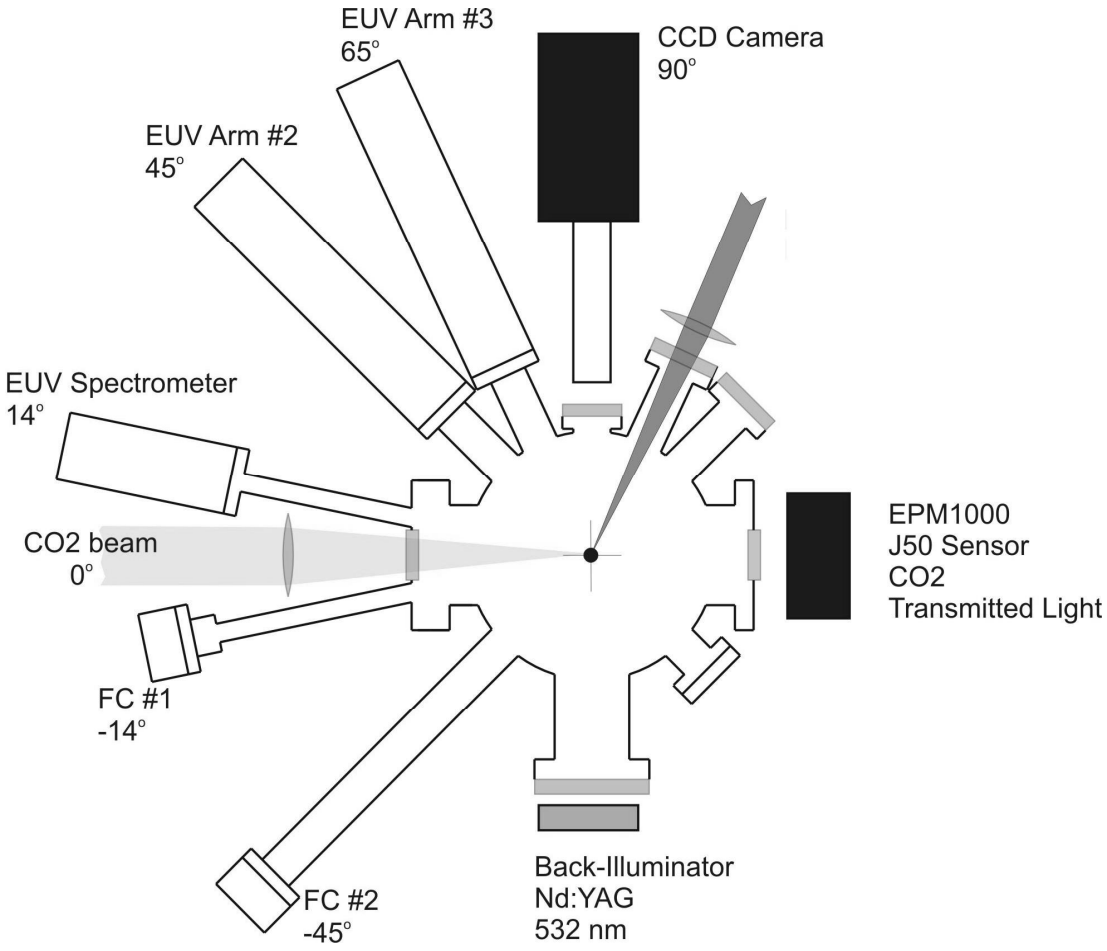

Figure 9. Low repetition rate experimental setup with diagnostic tools for CE optimization, EUV spectra and ion energy distribution measurements.

The apparatus is equipped with all required sub-systems (including droplet generator, back-illumination) and diagnostic tools. The diagnostics include two EUV energy measurement detectors (mounted at 45° and 65° with respect to the incident laser beam), an EUV spectrometer and two Faraday Cup detectors. The low repetition rate drive laser described earlier[2] was upgraded to produce up to 300 mJ of energy on target. The beam spot was characterized with a Spiricon detector in the far field zone. The beam waist size was about 100 μm in diameter in the focal plane.

Figure 10 shows measurements of CE for various positions of the focusing lens from the target using both EUV energy monitors. A double hump can be clearly observed in these curves, demonstrating that at these parameters the optimal intensity was reached and even exceeded. Figure 11 shows the dependence of conversion efficiency on laser peak intensity, obtained with laser pulses of about 300 mJ. The optimal intensity on target is at about 0.3 - 0.5 10^{10} W/cm^2. The maximum achieved CE on flat targets was in the range of 4.5 – 5 %.

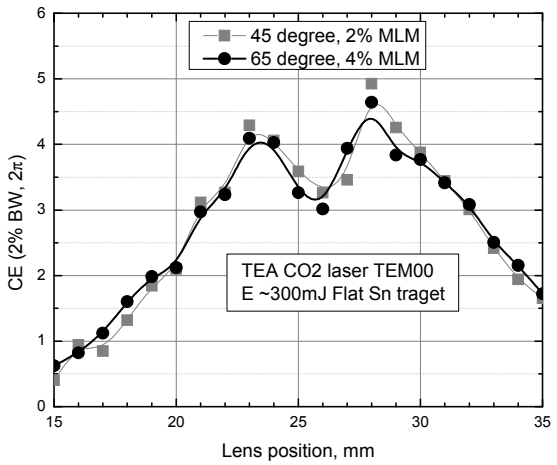

Figure 10. Variation of CE with the focusing lens position in front of flat target.

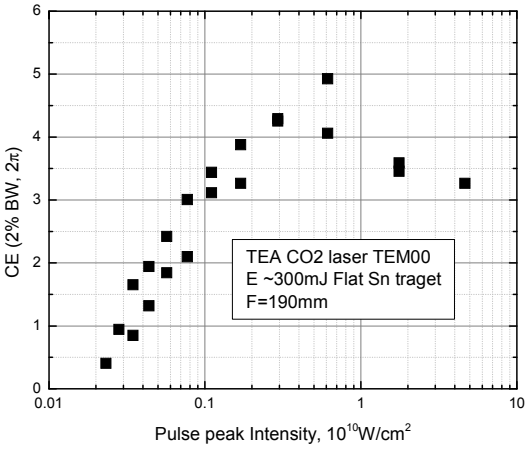

Figure 11. Dependence of CE on pulse peak intensity.

To record EUV spectra we used a grazing incidence flat-field spectrometer with a resolution better than 0.02 nm (the resolution varied from 0.011 nm to 0.016 nm for wavelengths from 8 nm to 20 nm)[6]. Using lithium and oxygen lines the spectrometer was calibrated with high accuracy (better than 2 pm). Figure 12 shows spectra for laser energies varied between 130 mJ and 320 mJ. It is found that for laser energies exceeding 180 mJ the spectra are almost identical in this energy range. For low intensities (energy <130 mJ) the center intensity of the spectrum is shifted towards longer wavelength radiation.

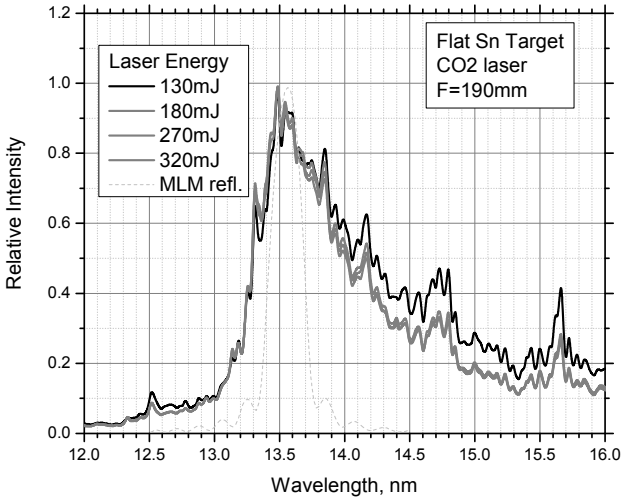

Figure 12. EUV spectra of Sn LPP with CO2 drive laser on flat target at various energies of incident radiation.

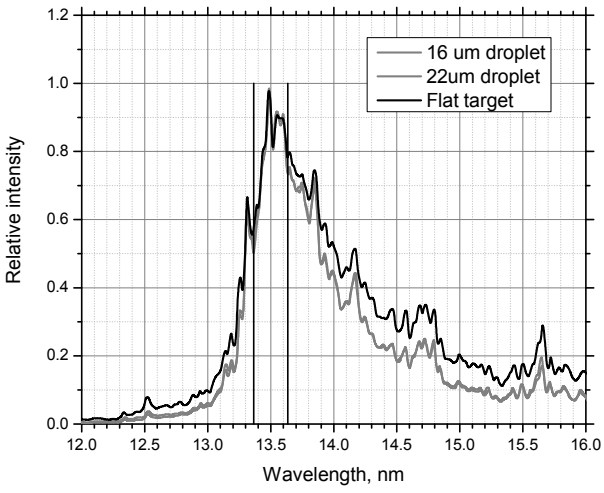

Figure 13. EUV spectra taken on flat target and small (16 μm and 22 μm) droplets.

Figure 13 shows a comparison of EUV spectra obtained on a flat target with those observed for small (16 μm and 22 μm diameter) droplets when a pre-pulse from a YAG-laser was used. It is found that the spectra show the same

features for droplets as for the flat target. However, the droplet spectra have higher spectral efficiency and are narrower compared to the spectrum for the flat target.

6. ION MEASUREMENTS

One of the important processes responsible for collector reflectivity degradation is sputtering of the collector by the high-energy ions generated from the plasma. Previously, we presented results on a protection technique developed by Cymer for attenuation of the ion flux and slowing down of the ions before reaching the collector[2]. These experiments were performed with a Faraday Cup (FC) detector installed at 45° with respect to the laser beam direction. The polar angles of EUV radiation and ion flux for an HVM collector are in the range from 16° to 80° (angles measured with respect to the laser beam). For characterization and optimization of the protection technique we conducted ion measurements at small (14°) and medium angle (45°). The goal of the characterization was to determine if the ion energy distribution at small angles differs significantly from the one at medium angles. At the same time we do not expect ion energy and flux to increase for angles larger than 45°.

The measurements were conducted on droplets at the conditions corresponding to high CE (about 3% in-band into 2π). The setup is shown schematically in Figure 9. Two Faraday Cup detectors (Kimball Physics, FC-73A) for ion energy distribution measurements are mounted at the angles of 14° and 45° at a distance of 43-46 cm from plasma.

The FC detectors were configured for ion detection by applying a negative voltage of 30-50 V to the suppression grid to reduce the influence of secondary electrons emitted from the collector (see Figure 15). The collector was loaded with a resistor of 1 kΩ. For simple measurements the retarding grid of the FC was grounded. For ions of the same charge state Z the FC waveform signal $U_i(t_i)$ is proportional to the absolute velocity distribution of ions $\varphi(v)$, where the velocity is defined by the time of flight t_i and distance from plasma to the FC collector *L*. In our case we have ions with various Z, thus the signal should be normalized to the Z- state (or average Z), because ions carry the charge proportional to the Z. For conversion of the FC signal into the energy distribution function $f(\varepsilon)$ we converted velocity into kinetic energy, assuming that all ions have a mass of *M*=118.7 a.u. The FC voltage signal U_i is proportional to the absolute velocity distribution function and should be multiplied by the derivative of velocity by energy for proper conversion into the energy distribution function. After simple transformations, we obtain that the conversion is just given by the multiplication of voltage by time-of-flight:

$$f(\varepsilon) = \varphi(v(\varepsilon)) \cdot \frac{dv}{d\varepsilon} = \varphi(v(\varepsilon)) \frac{1}{\sqrt{2M\varepsilon}} \quad \text{where} \quad v(\varepsilon) = \sqrt{\frac{2\varepsilon}{M}}$$

$$v_i = \frac{L}{t_i}; \qquad \varphi(v_i) \propto U_i(t_i) \qquad f(\varepsilon_i) \propto U_i t_i \qquad \varepsilon_i = \frac{M v_i^2}{2}$$

The typical ion energy distribution functions obtained from processed FC waveforms are shown in Figure 14 for two angles (14° and 45°). The maximum energy observed at the small angle (E_{max}=3.5 keV) is slightly higher than the one observed at 45° angle (E_{max}=3.0 keV). The peak of the energy distribution is at E_{peak} = 2.0 keV for small angles and E_{peak} = 1.6 keV for 45°. The ion flux at small angle is approximately 2 times less compared to the one at 45°, although the diagnostic tools were identical (same apertures, distances, schematics).

Measurements on characterization of the ion states were conducted on flat targets using the FC detector. A retarding potential was applied to the retarding grid of the FC (see Figure 15), and the recorded waveforms were processed according to the algorithm described above. The original waveforms had a saw-tooth-like shape at high times-of-flight, corresponding to low ion velocities. When the waveforms were converted into the ion energy distributions, the saw-tooth structure revealed well-distinguished low energy cut-off edges corresponding to ions of various Z states. The edge position is equal to the retarding potential multiplied by the Z number (*Z*=1, 2, etc.).

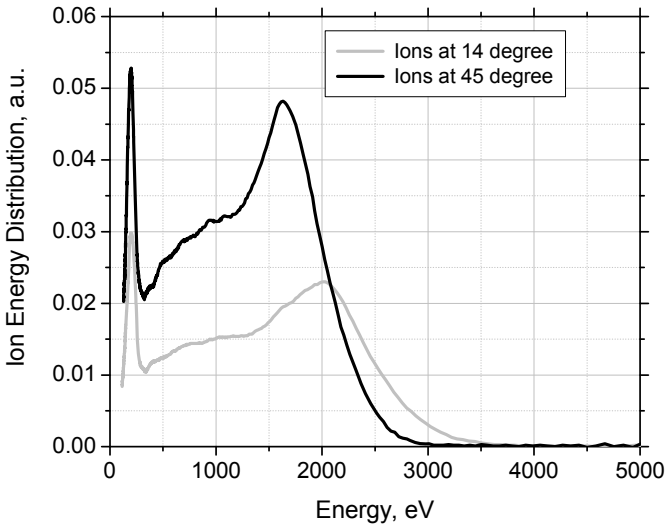

Figure 14. Measurements of Ion Energy distributions at 14 and 45 degrees with respect to the laser beam.

The ion energy distributions for two different retarding grid voltages are shown in Figure 16. Ions with charge Z up to 7 can be distinctly observed. In order to obtain the number of ions for a given Z the presented distribution should be divided by Z. This type of processing is complicated by the influence of neighboring ion states. Information about Z- states of the ions coming from the plasma is an important part of the optimization of the debris protection techniques.

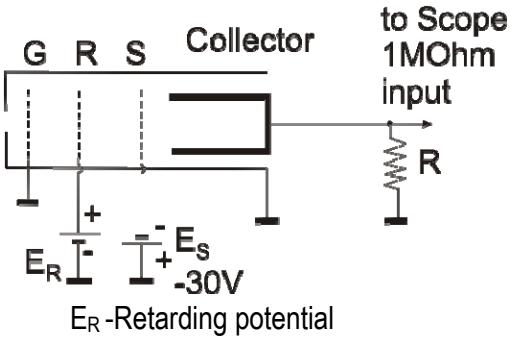

Figure 15. Schematic of Faraday Cup measurement tool.

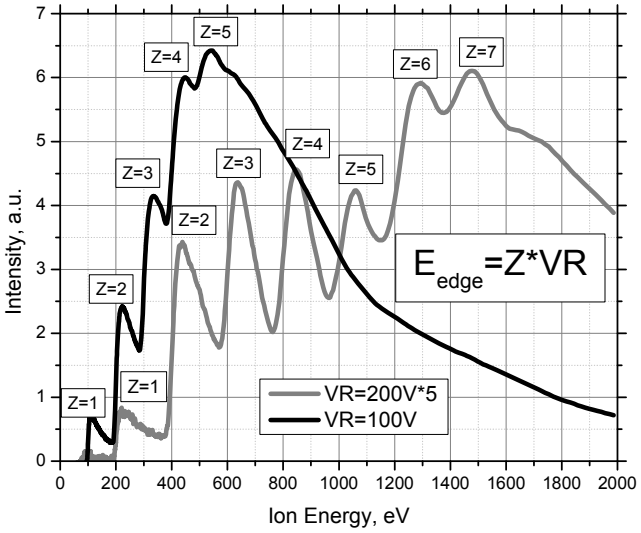

Figure 16. Ion Charge State measurements. Waveform converted into energy scale shows cut-off edges of ions with different Z. Ions with Z=7 and below are well distinguished.

7. CONCLUSIONS

A laser-produced plasma EUV source has been shown to be the most viable light source technology with high scalability to meet requirements from leading scanner manufacturers and provide a path towards higher power as the lithography tools evolve over their life cycle. Progress achieved on the development of subsystems described in this

paper enabled us to demonstrate high stability of EUV energy during extended source operation times at high average power. Debris mitigation techniques were tested with a 1.6sr collector revealing no erosion of the Mo/Si layers for 8 hours of operation and demonstrating promising protection results during a run for more than 50 hours. Optimal beam intensity was measured with a high-energy drive laser. EUV spectra were measured at various laser intensities on flat and droplet targets. Characterization of ions generated by the plasma was performed at small angles. Separation of ions with different charge states was demonstrated with FC diagnostics. These investigations were aimed at optimization of the debris mitigation techniques and protection of the collector. Cymer is committed to commercializing an HVM EUV light source for the sub-32nm node and continues to meet its EUV source development schedule. Integrated system testing with 320mm (1.6sr) collector has shown stable transmission of EUV power to IF and good distribution of EUV energy in the far field. EUV lithography is expected to be the critical-dimension imaging solution for post-193 nm immersion tools. LPP source technology is the most viable solution to enable the IF power requirement projected in the future and to provide the much needed margin in photoresist sensitivity, optics degradation, process latitude, and overall equipment throughput. The laser-produced plasma technology is our chosen technology path for HVM EUV lithography applications.

8. ACKNOWLEDGEMENTS

The authors gratefully acknowledge the valuable contributions from Martin J. Neumann and David N. Ruzic of University of Illinois, Urbana Champaign, Marco Perske, Hagen Pauer, Mark Schürmann, Sergiy Yulin, Torsten Feigl and Norbert Kaiser of Fraunhofer Institut f. Angewandte Optik und Feinmechanik, Eric Gullikson and Farhad Salmassi of Lawrence Berkeley National Laboratory, Frank Scholze, Christian Laubis, Christian Buchholz and coworkers at PTB, Steven Grantham and Charles Tarrio of the National Institute of Standards and Technology, and Mark Tillack and Yezheng Tao of the University of California at San Diego. We are also very thankful for the invaluable support and contributions, past and present, of many scientists, engineers and technicians involved in the EUV technology program at Cymer.

REFERENCES

1. K. Ota, Y. Watanabe, V. Banine, H. Franken, in: "EUV Sources for Lithography", Edt. Vivek Bakshi, (SPIE Press, Bellingham, WA 2005), Chapter 2, p 27 – 43.

2. I. V. Fomenkov, D. C. Brandt, A. N. Bykanov, A. I. Ershov, W. N. Partlo, D. W. Myers, N. R. Böwering, G. O. Vaschenko, O. V. Khodykin, J. R. Hoffman, E. Vargas L., R. D. Simmons, J. A. Chavez, C. P. Chrobak. "Laser-produced plasma source system development" in *Emerging Lithographic Technologies XI*, edited by Michael J. Lercel, Proc. of SPIE Vol. **6517** (SPIE, Bellingham, WA, 2007) 6517 3J.

3. N. R. Böwering, A. I. Ershov, W. F. Marx , O. V. Khodykin, B.A.M. Hansson, W. N. Partlo, E. Vargas L., J. A. Chavez, I. V. Fomenkov, D. W. Myers, D. C. Brandt, "EUV Source Collector", in *Emerging Lithographic Technologies X*, edited by M. J. Lercel, Proc. of SPIE Vol. **6151** (SPIE, Bellingham, WA, 2006) 61513R.

4 D. C. Brandt, I. V. Fomenkov, A. I. Ershov, W. N. Partlo, D. W. Myers, N. R. Böwering, A. N. Bykanov, G. O. Vaschenko, O. V. Khodykin, J. R. Hoffman, E. Vargas L., R. D. Simmons, J. A. Chavez, C. P. Chrobak, "LPP EUV Source Development for HVM", in *Emerging Lithographic Technologies XI*, edited by M. J. Lercel, Proc. of SPIE, Vol. **6517-25** (SPIE, Bellingham, WA, 2007).

5. D. C. Brandt, I. V. Fomenkov,, A. I. Ershov, W. N. Partlo, D. W. Myers, N. R. Böwering, G. O. Vaschenko, O. V. Khodykin, A. N. Bykanov, J. R. Hoffmann, C. P. Chrobak, S. N. Srivastava, D. A. Vidusek, S. De Dea, R. R. Huo "Laser-produced plasma source system development" in: *Lithography Asia 2008,* Proc. SPIE Vol. **7140** (SPIE, Bellingham, WA, 2008) 71401E.

6. N. R. Böwering, J. R. Hoffman, O. V. Khodykin, C. L. Rettig, B. A. M. Hansson, A. I. Ershov, I. V. Fomenkov, "Metrology of laser-produced plasma light source for EUV lithography", in *Metrology, Inspection, and Process Control for Microlithography XIX*, edited by Richard M. Silver, Proc. of SPIE Vol. **5752** (SPIE, Bellingham, WA, 2005) 1248-1256.